

Journal of Materials Chemistry A

Accepted Manuscript



This is an *Accepted Manuscript*, which has been through the Royal Society of Chemistry peer review process and has been accepted for publication.

Accepted Manuscripts are published online shortly after acceptance, before technical editing, formatting and proof reading. Using this free service, authors can make their results available to the community, in citable form, before we publish the edited article. We will replace this *Accepted Manuscript* with the edited and formatted *Advance Article* as soon as it is available.

You can find more information about *Accepted Manuscripts* in the [Information for Authors](#).

Please note that technical editing may introduce minor changes to the text and/or graphics, which may alter content. The journal's standard [Terms & Conditions](#) and the [Ethical guidelines](#) still apply. In no event shall the Royal Society of Chemistry be held responsible for any errors or omissions in this *Accepted Manuscript* or any consequences arising from the use of any information it contains.

Cite this: DOI: 10.1039/c0xx00000x

www.rsc.org/xxxxxx

ARTICLE TYPE

Converting “real-world” mixed waste plastics into porous carbon nanosheet with excellent performance in adsorption of organic dye from wastewater†

Jiang Gong,^{a,b} Jie Liu,^a Xuecheng Chen,^{a,c} Zhiwei Jiang,^a Xin Wen,^a Ewa Mijowska^c and Tao Tang^{*a}

Received (in XXX, XXX) Xth XXXXXXXXX 200X, Accepted Xth XXXXXXXXX 200X
DOI: 10.1039/b000000x

Waste plastic utilization and wastewater treatment are the two most serious challenges on the way of urbanization and industrialization due to the limited fossil fuel resource, ever-increasing energy demand and severe environmental pollution. Conversion of waste plastics into high value-added carbon nanomaterials has become a promising way to utilize waste plastics; however, most of current studies are limited to single component waste plastic; besides, little attention has been paid to porous carbon nanosheet (PCNS). Herein, a facile approach was established to prepare PCNS by carbonization of “real-world” mixed waste plastics on organically-modified montmorillonite and the subsequent KOH activation. The morphology, microstructure, textural property, phase structure, surface element composition and thermal stability of PCNS were investigated. PCNS showed high specific surface area (2315 m²/g) and large pore volume (3.319 cm³/g) with high purity (>99.6%). More importantly, PCNS exhibited fast adsorption (about 95% of methylene blue (MB) was removed during the first 10 min of adsorption), unprecedented adsorption capacity of 769.2 mg/g (higher than most of reported adsorbents) and excellent recyclability (after ten cycles, adsorption capacity of 692.0 mg/g was remained, and 90 wt % of PCNS was reclaimed) for MB from wastewater. This was attributed to the high specific surface area and large pore volume of PCNS, and multiple adsorption mechanisms including pore filling, hydrogen bonding, π - π and electrostatic interactions between MB and PCNS. It is believed that this work not only provides a novel potential way to utilize waste plastics, but also puts forward a facile sustainable approach to synthesize PCNS, which will be an ideal candidate for various applications.

1. Introduction

Owing to the global scale of severe water pollution arising from industrial pollutants, the creation of efficient absorbent materials for separation and removal of pollutants from wastewater is of utmost importance to address environmental issues.¹⁻¹⁰ Adsorption of organic dyes using adsorbents is generally low-cost and versatile, and represents one of the most widely used methods for removing organic dyes from wastewater.¹¹⁻¹⁵ A variety of efficient absorbents, including carbon nanotube (CNT),¹⁶ graphene,¹⁷ activated cup-stacked CNT (CS-CNT),¹⁸ Ni/C nanomaterial,¹⁹ BN hollow sphere,²⁰ Ni nanosphere,²¹ porous MnO₂ microsphere,²² montmorillonite,²³ activated CNT,²⁴ activated carbon,²⁵ ordered mesoporous carbon,^{26,27} carbon nanofiber (CNF) aerogel²⁸ and carbonaceous nanofiber membrane,²⁹ have been employed for adsorption of organic dyes from wastewater. Particularly, activated carbon with huge surface area is extensively applied due to its high efficiency for the removal of pollutants; however, it shows some drawbacks such as the slow adsorption kinetics, poor selectivity and limited working capacity for the removal of large-sized molecules.

Recently, carbon nanosheet (CNS), a two-dimensional carbon

nanostructure of stacked graphene sheets with few nanometers thickness, has received considerable research interest because of its high surface area, developed porous structure, abundant surface functional groups, and good chemical and thermal stabilities, and its potential applicability in various fields such as adsorption,³⁰ energy storage,³¹ organic transistor³² and oxygen reduction reaction.³³ Compared to activated carbon, the much smaller thickness of CNS enables the fast adsorption kinetics and a high utilization degree of the overall porosity and surface area. Additionally, the aggregation or restacking inevitably occurring in graphene assemblies which results in significant compromise or degradation of the unique properties of individual sheets can be avoided in the CNS, thanks to its weaker intersheet van der Waals attraction than graphene. As a consequence, the particular physicochemical properties make CNS an ideal absorbent for environment remediation.

On the other hand, as we know, plastics have become an essential part of our modern lifestyle, and the world production of plastics increased from 1.7 million tons in 1950 to 288 million tons in 2012. Correspondingly, more than 25 million tons of waste plastics were generated in 2012 in Europe.³⁴ The ever-increasing generation of waste plastics has created terrible

environment issues and aggravated the energy crisis, because most of plastics are not biodegradable and originate from the unsustainable fossil fuels. Sustaining development and the growing global demands for energy, chemicals and materials have fostered research efforts to exploit renewable raw materials to reduce the dependency on the limited fossil fuels^{35–41} or develop low environmental impact technologies for the sustainable recycling of waste plastics in place of the current practice of incineration and landfilling.^{42,43} Mechanical recycling of waste plastics is far from being widely accepted by the population because of the low quality of the recycled plastic mixture. Chemical recycling can recover the petrochemical components from waste plastics to produce monomers, fuels, gases and other useful chemicals.^{44,45} However, the development of facile, economically feasible, sustainable approaches to largely transform waste plastics into high value-added products is extremely important to be competitive and stimulate the utilization progress of waste plastics.

Since most of plastics contain a high content of carbon element, special attention has been focused on the utilization of waste plastics, including polypropylene (PP), polyethylene (PE) and polystyrene (PS), to synthesize valuable carbon nanomaterials (CNMs) such as CNT, CS-CNT, CNF, carbon sphere (CS), hollow CS (HCS) and graphene.^{46–59} For example, Wu et al. catalyzed gasification of waste PP and PS into CNTs using Ni-Mn-Al catalyst;⁴⁶ however, the quality of CNTs needed to be improved. Zhuo et al. synthesized CNTs from recycled PE using stainless-steel wire mesh as catalyst by a pyrolysis-combustion technique;⁴⁸ unfortunately, the yield of CNTs was low (about 10%). Pol et al. used autoclave as reactor to convert PP and PS into CNTs and CSs, which showed high performance in lithium electrochemical cells,⁴⁹ but the high pressure nature of autoclave was not in favor of massive and continuous production. Ruan et al. converted waste PS into high quality graphene using a Cu foil as template by chemical vapor deposition.⁵² Our group found that the combination of solid acid (or halogenated compound, or activated carbon) with nickel (or cobalt) catalyst could convert PP, PE and PS into CNTs, CS-CNTs, CNFs and HCSs with high yield under atmospheric conditions.^{53–59} Unfortunately, most of current studies are limited to single component waste plastic and no studies involving “real-world” mixed waste plastics which mainly consist of PP, PE and PS⁶⁰ have been reported. Therefore, converting “real-world” mixed waste plastics into high value-added CNMs with controlled morphology and high yield is of great significance for comprehensive utilization of the large amount of waste plastics.

In this work, “real-world” mixed waste plastics, which consisted of PP from waste woven bags (Fig. 1a), PE from waste vessels (Fig. 1b) and PS from waste foam sheets (Fig. 1c), were effectively transformed into CNS on organically-modified montmorillonite (OMMT). Compared to other common carbon sources for the synthesis of CNS such as hexachloroethane,³⁰ polyaniline,³¹ pitch,^{32,61} folic acid,³³ methane,⁶² ladder-like compound,⁶³ phenol-formaldehyde resin,⁶⁴ resorcinol-formaldehyde resin,^{65–67} acetylene,⁶⁸ glycerol and melamine,⁶⁹ reutilization of “real-world” mixed waste plastics to synthesize CNS not only shows advantages with cheap and abundant sources, and environmentally friendly and cost-effective methods,

but also contributes to sustainable development and relieves the energy crisis. More importantly, after KOH activation, porous CNS (PCNS) with high specific surface area (2315 m²/g) and large pore volume (3.319 cm³/g) was synthesized, which was demonstrated to show fast adsorption, unprecedented adsorption capacity (769.2 mg/g, higher than most of reported adsorbents) and excellent recyclability for removal of methylene blue (MB) from wastewater.

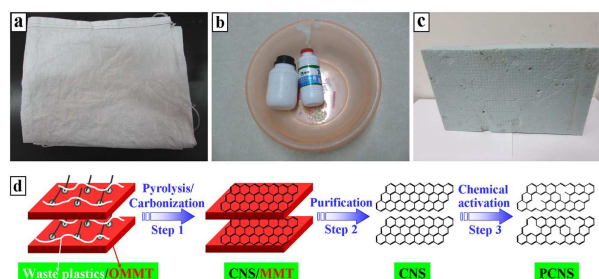


Fig. 1 Digital images of ubiquitous waste plastics: PP woven bags (a), PE vessels (b) and PS foam sheets (c). Schematic illustration for the process of synthesizing PCNS from the “real-world” mixed waste plastics (d).

2. Experimental

2.1 Materials

The “real-world” mixed waste plastics (Figs. 1a–1c) were washed and cut into small pieces before being used. OMMT (Closite 15A, organic modifier: dimethyl-dihydrogenated tallow quarternary ammonium, and modifier concentration: 125 mequiv per 100 g clay) was purchased from Southern Clay. MB was of analytical grade quality and supplied by Alfa Aesar. All other chemicals were of analytical-grade quality. All solutions were prepared using deionized water and analytical-grade chemicals to eliminate the impurities including oxidation substances.

2.2 Preparation of PCNS

The “real-world” mixed waste plastics (15.00 g) consisting of PP (26.9 wt %, 4.04 g), PE (56.3 wt %, 8.45 g) and PS (16.8 wt %, 2.51 g) according to previous work⁶⁰ were mixed with OMMT at a weight ratio of 1/4 in a Brabender mixer at 100 rpm and 190 °C for 5 min. CNS/OMMT composite was firstly synthesized by carbonizing the resultant mixed waste plastics/OMMT composite (Fig. 1d, step 1) in a conventional quartz tube reactor with an internal diameter of 60 mm at 700 °C under N₂ atmosphere (Fig. S1 in the ESI†). Previous study demonstrated that OMMT not only promoted the degradation of mixed plastics into aromatics and light hydrocarbons, but also catalyzed these degradation products into CNS through polymerization mechanism.⁷⁰ Subsequently, after purifying CNS/OMMT composite by hydrofluoric acid and nitric acid (Fig. 1d, step 2), 9.10 g of CNS was obtained, and then mixed with KOH at a weight ratio of 1/6 and chemically activated at 850 °C for 1.5 h under Ar atmosphere. The resultant product was washed with 15 wt % HCl solution and deionized water to neutral condition, and finally dried at 120 °C for 12 h (Fig. 1d, step 3) to prepare PCNS (6.47 g).

2.3 Characterization

The morphologies of CNS and PCNS were observed by field-emission scanning electron microscope (FE-SEM, XL30ESEM-FEG). The microstructures of CNS and PCNS were investigated using transmission electron microscope (TEM, JEM-1011) at an accelerating voltage of 100 kV and high-resolution TEM (HRTEM) on a FEI Tecnai G2 S-Twin transmission electron microscope operating at 200 kV. The phase structures of CNS and PCNS were analyzed by X-ray diffraction (XRD) using a D8 advance X-ray diffractometer with Cu K α radiation operating at 40 kV and 200 mA. Raman spectroscopy (T6400, excitation-beam wavelength: 514.5 nm) was used to characterize the vibrational properties of CNS and PCNS. The textural properties of CNS and PCNS were measured by nitrogen adsorption/desorption at 77 K using a Quantachrome Autosorb-1C-MS analyzer. The specific surface area was calculated by Brunauer-Emmett-Teller (BET) method. The surface element compositions of CNS and PCNS were characterized by means of X-ray photoelectron spectroscopy (XPS) carried out on a VG ESCALAB MK II spectrometer using an Al K α exciting radiation from an X-ray source operated at 10.0 kV and 10 mA. The thermal stabilities of CNS and PCNS were measured by thermal gravimetric analysis (TGA) under air flow at a heating rate of 10 °C/min using a TA Instruments SDT Q600. The functional groups of PCNS before and after MB adsorption, and pure MB were characterized by Fourier-transform infrared spectroscopy (FT-IR, Bio-Rad FTS-135).

2.4 Adsorption experiment

Adsorption experiment of MB using CNS or PCNS was carried out in a batch process by stirring 25.0 mg CNS or PCNS in 50.0 mL of MB solution in 100-mL polyethylene flask. The equipment was exposed in normal slight white light source, which was far away from UV light. Working solution of MB was prepared from the stock solution (1000 mg/L) to the desired concentration for each experimental run. The pH of MB solution was adjusted to 6 by 0.5 mol/L HCl solution. After stirring for 180 min, 1.0 mL of MB solution was withdrawn by a syringe, diluted, and filtered through 0.25 μ m membrane for later analysis of MB concentration. The absorbance of MB solution was measured by UV/Vis/NIR spectrophotometer (Lambda 900) to monitor the absorbance at $\lambda_{\text{max}} = 665 \pm 1$ nm, corresponding to the maximum absorbance. The concentration of MB solution was determined by linear regression equation obtained by plotting the calibration curve for MB over a range of concentrations.

3. Results and discussion

3.1 Morphology and microstructure

FE-SEM and TEM observations are conducted to characterize the morphologies of CNS and PCNS. FE-SEM images of CNS and PCNS depicted the layered morphology consisting of thin, leaf-like nanosheets ranging from hundreds of nanometers to several micrometers in length (Figs. 2a and 2b). TEM analyses verified the sheets like-arrangement of CNS with randomly arranged wrinkled structure and rough surface (Fig. 2c). Likewise, PCNS maintained a crumbled thin sheet structure (Fig. 2b), but its surface was obviously rougher than that of CNS (Fig. 2d). HRTEM is used to further study the microstructures of CNS and

PCNS. A slight degree of ordering was observed in the CNS (Figs. 3a and 3b), which revealed its low graphitization degree. After KOH activation, porous structure with several to a dozen of nanometers was formed in the PCNS (Fig. 3c), similar to porous graphene activated by KOH as reported previously,⁷¹ indicating that this activation process was able to etch graphitic layers to generate porous structure.

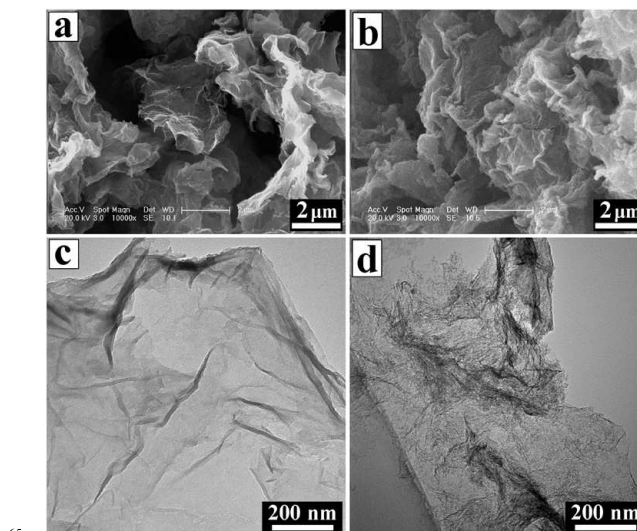


Fig. 2 FE-SEM and TEM images of CNS (a and c) and PCNS (b and d).

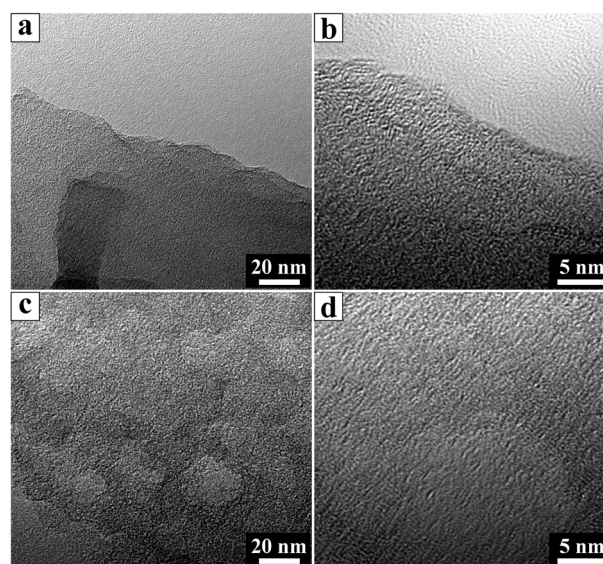
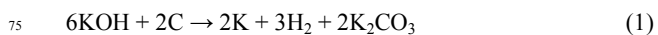


Fig. 3 HR-TEM images of CNS (a and b) and PCNS (c and d).

The activation mechanism is normally suggested to include independent hydroxide and redox processes during the reaction. With the activation treatment, KOH powder can react with carbon as follows:⁷²



When the temperature is higher than 700 °C, the reaction proceeds as follows:





When the temperature is higher than 800 °C, the reaction proceeds as follows:



The etched pores played the crucial roles in the adsorption process of dye, not only as diffusive channels but also as active sites for adsorption capacity enhancement because of pore edges. Thereby, it is expected that the synthesized PCNS may be used as an adsorbent in environment remediation. Moreover, PCNS exhibited slightly serrated edges and showed randomly oriented lattice fringes comparing with CNS, which indicated that the stacking of graphene layers in the PCNS became a little more disordered (Fig. 3d).

3.2 Textural property, phase structure, surface element composition and thermal stability

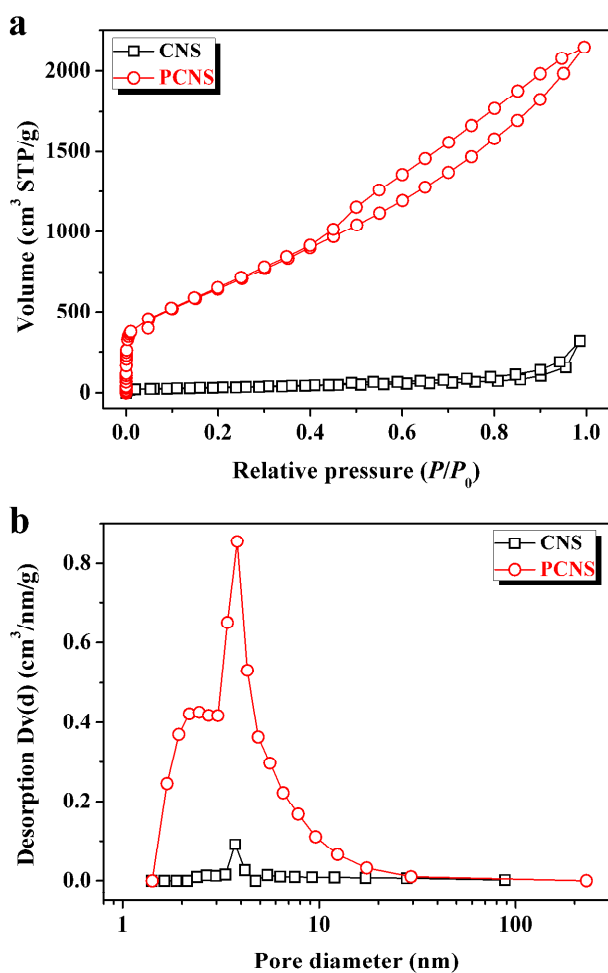


Fig. 4 Nitrogen adsorption/desorption isotherms (a) and pore size distributions (b) of CNS and PCNS.

To analyze the textural properties of CNS and PCNS, nitrogen adsorption/desorption measurements are carried out at 77 K. It was evident that PCNS presented the combined type I/IV physisorption isotherm (Fig. 4a). A high adsorption capacity was observed at low relative pressure ($P/P_0 < 0.1$), which indicated

the presence of a lot of micropores in the PCNS. The type-H4 hysteresis loop at a relative pressure P/P_0 ranging from 0.4 to 1.0, which resulted from the filling and emptying of mesopores by capillary condensation, demonstrated the formation of a large number of mesopores in the PCNS. The BET surface area (S_{BET}) and pore volume (V) of PCNS were calculated to be 2315.0 m^2/g , which is close to the theoretical value of graphene (2650 m^2/g), and 3.319 cm^3/g , respectively. Compared with CNS (113.4 m^2/g and 0.492 cm^3/g), the large S_{BET} and V enhancements of PCNS were attributed to KOH activation, which was a very efficient method to etch pores and increase the content of defective and edge sites. The pore size distributions were calculated using the Barrett–Joyner–Halenda model from the desorption branches of the isotherms. As shown in Fig. 4b, PCNS mainly exhibited a narrow pore size distribution with an average diameter (D_{AV}) of about 3.8 nm, which was in good agreement with the pore size observed from HRTEM image.

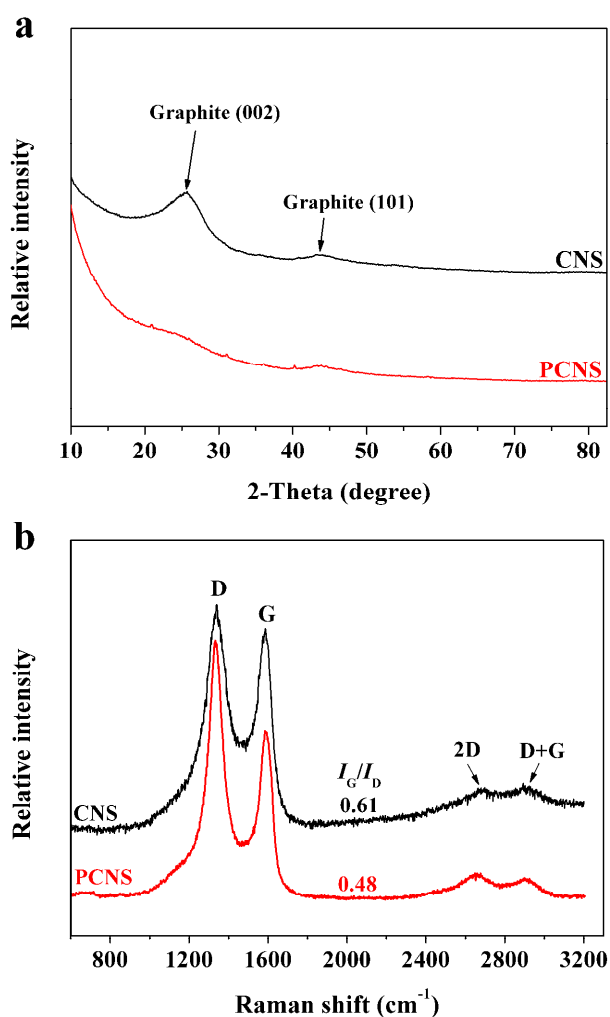


Fig. 5 XRD patterns (a) and Raman spectra (b) of CNS and PCNS.

To investigate the phase structures of CNS and PCNS, XRD characterization is employed (Fig. 5a). The appearance of two broad and weak diffraction peaks at $2\theta = 26.3^\circ$ and 43.2° , which were assigned to the typical graphitic (002) and (101) planes,⁷³

respectively, revealed the low graphitization degree of CNS. The absence of the characteristic peak of pristine graphite at $2\theta = 26.3^\circ$ reflected the amorphous nature and irregular arrangement of carbon layers in the obtained PCNS, which was consistent with HRTEM observation. Raman spectroscopy is further used to gain more insights into the phase structure information of CNS and PCNS (Fig. 5b). The D band at 1350 cm^{-1} and G band at 1580 cm^{-1} are related to the disordered and defective structure of carbon material and the ordered carbon structure with sp^2 electronic configuration, respectively. It is well known that the intensity ratio of G/D peak (I_G/I_D) is often applied to estimate the degree of perfection of graphene planes.⁵⁶ After KOH activation, the I_G/I_D value decreased from 0.61 for CNS to 0.48 for PCNS, which resulted from the generation of many defects during KOH activation. Besides, the negligible 2D band at about 2660 cm^{-1} and D+G band at about 2880 cm^{-1} verified the amorphous nature and multilayer of both CNS and PCNS.⁷⁴

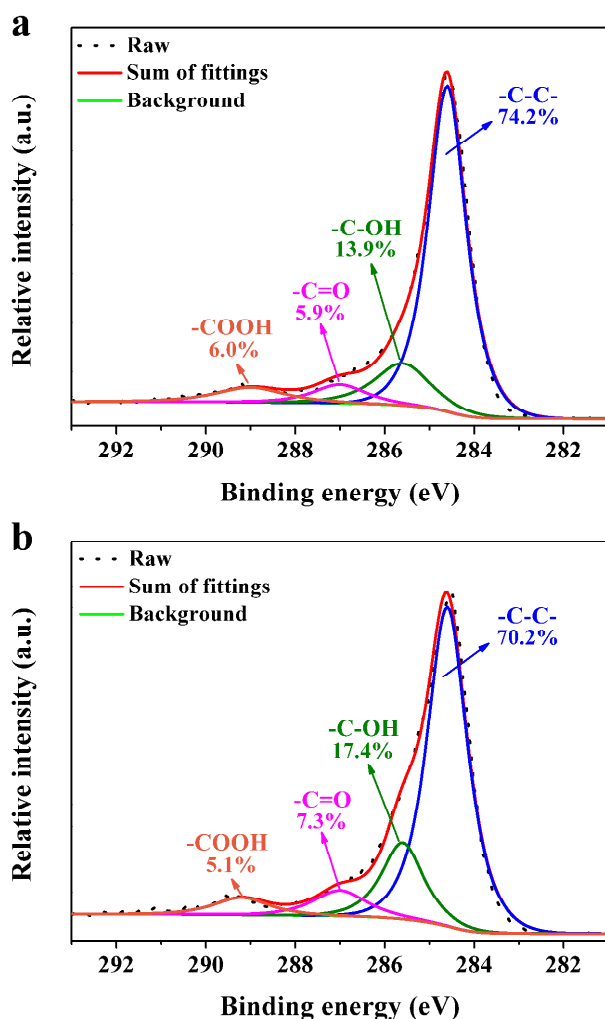


Fig. 6 C 1s high-resolution XPS spectra of CNS (a) and PCNS (b).

XPS measurements are carried out to get the detailed bonding information and quantify the elemental atom ratios in the CNS and PCNS. Fig. S2 shows the survey scan spectra with apparent C 1s (284.6 eV) and O 1s (532.3 eV) peaks. The high-resolution

C1s XPS spectra are curve-fitted into four individual peaks: graphitic carbon ($284.4\text{--}284.6\text{ eV}$), -C-OH ($285.6\text{--}285.7\text{ eV}$), -C=O ($286.7\text{--}287.0\text{ eV}$) and -COOH ($288.7\text{--}289.0\text{ eV}$),⁷⁵ as displayed in Fig. 6. Comparing with CNS, PCNS possessed relatively higher oxygen content and more surface functional groups including -C-OH and -C=O , which facilitated the removal of heavy metallic ions or cationic dyes from wastewater.⁷⁶ TGA and the derivate TGA (DTG) are used to evaluate the graphitic nature and purity of CNS and PCNS (Fig. 7). The first weak region of weight loss from 100 to $400\text{ }^\circ\text{C}$ was attributed to the release of chemisorbed water and the pyrolysis of oxygen-containing functional groups. A remarkable weight loss occurred between 400 and $700\text{ }^\circ\text{C}$, which was ascribed to the oxidation of carbon skeleton of graphene sheets. The lower maximum oxidation temperature of PCNS ($519.3\text{ }^\circ\text{C}$) than that of CNS ($572.1\text{ }^\circ\text{C}$) demonstrated the formation of a lot of defects and/or oxygen-containing functional groups by KOH activation. The residues of CNS and PCNS at $800\text{ }^\circ\text{C}$ were less than 0.4% , indicating that CNS and PCNS had high purity.

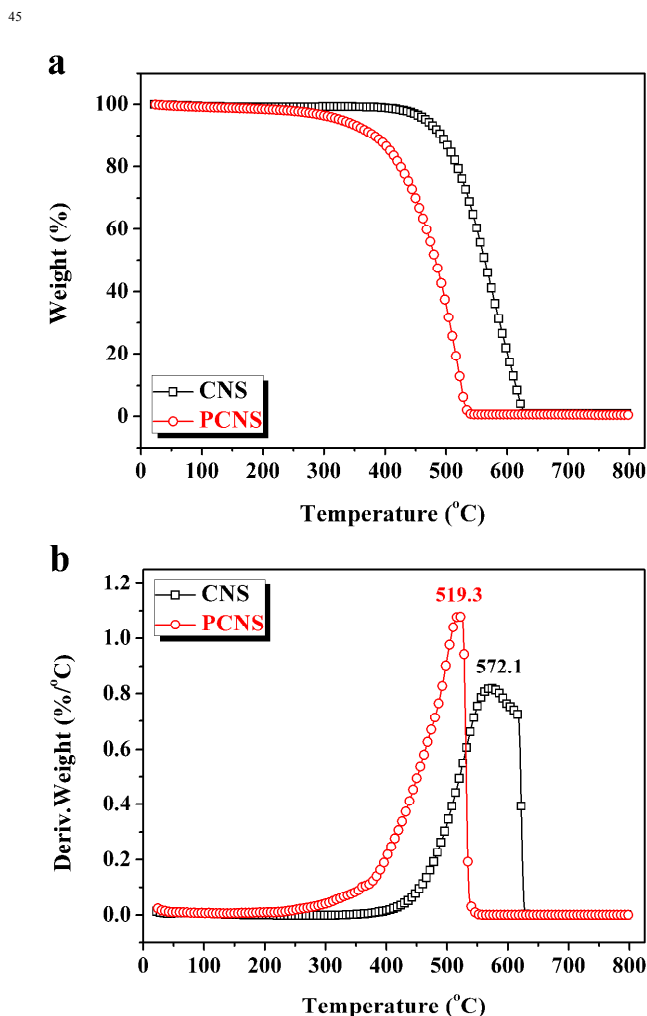


Fig. 7 TGA (a) and DTG (b) curves of CNS and PCNS under air flow at $10\text{ }^\circ\text{C}/\text{min}$.

3.3 Application in adsorption of MB

In the above results, “real-world” mixed waste plastics were

catalyzed into PCNS with high S_{BET} , large V as well as abundant surface functional groups using a facile sustainable approach. It is very attractive for academic and industrial communities to explore its potential applications in the environment remediation, energy storage and catalysis, *etc.* In this work, as an example, PCNS was utilized for adsorption of MB from wastewater. Our previous studies showed that the removal efficiency of MB by PCNS in normal slight white light was very close to that in the dark environment or under UV light (Fig. S3). This demonstrated that the photo-degradation of MB by PCNS under our experimental conditions could be neglected and the removal of MB resulted from the adsorption.

The equilibrium isotherm describes how the adsorbent interacts with the adsorbate, and the correlation of experimental result to adsorption model can help to understand the adsorption mechanism. Langmuir model is employed to represent the relationship between the equilibrium adsorption capacity (q_e , mg/g) of MB on the CNS (or PCNS) and its equilibrium solute concentration (C_e , mg/L) as follows:

$$q_e = q_m K_L C_e / (1 + K_L C_e) \quad (6)$$

where q_m is the maximum adsorption capacity (mg/g) corresponding to complete monolayer covering of MB, which depends on the number of adsorption sites, and K_L is the Langmuir constant (L/mg).

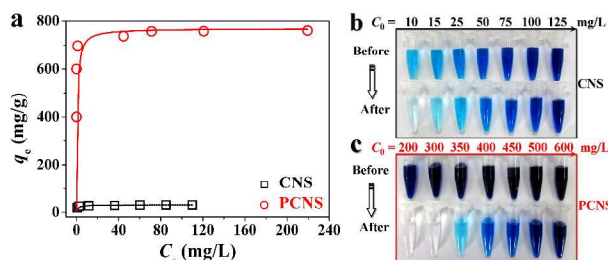


Fig. 8 (a) Equilibrium adsorption isotherms of MB on the CNS and PCNS (Experimental conditions: MB concentration = 10–125 mg/L for CNS or 200–600 mg/L for PCNS, CNS or PCNS concentration = 0.5 g/L, and adsorption time = 180 min), and the corresponding photos of the MB solutions before and after adsorption by (b) CNS, or (c) PCNS.

Table 1 Langmuir isotherm parameters of CNS and PCNS.

Parameter	CNS	PCNS
q_m (mg/g)	30.3	769.2
K_L (L/mg)	0.72	3.25
R^2	0.9994	0.9999

Fig. 8a shows the equilibrium adsorption isotherms of MB on the CNS and PCNS. The isotherms belonged to type I curve, which is characteristic of Langmuir isotherm. That is to say, the amount of adsorbed MB dramatically increased at a lower final solution concentration, suggesting a high affinity between MB molecules and PCNS surface. The adsorbed amount then reached a plateau at a higher equilibrium solution concentration, reflecting the saturated adsorption. As shown in Table 1, the R^2 value exceeded 0.999, meaning that Langmuir model fitted well

the experimental result. The q_m of PCNS for MB was as high as 769.2 mg/g, which was more than 24 times higher than that of CNS (30.3 mg/g). More importantly, compared to other reported adsorbents (Table 2), including graphene,¹⁷ activated CS-CNT,¹⁸ Ni/C nanomaterial,¹⁹ BN hollow sphere,²⁰ Ni nanosphere,²¹ porous MnO₂ microsphere,²² montmorillonite,²³ activated CNT,²⁴ activated carbon,²⁵ CNS,⁶⁹ ordered mesoporous carbon,²⁶ and CNF aerogel,²⁸ it could be clearly seen that PCNS showed an excellent adsorption performance of MB. Additionally, optical photographs are taken before and after MB adsorption (Figs. 8b and 8c). For example, after the adsorption of MB with an initial concentration of 300 mg/L on the PCNS, the polluted water became clear and colourless. This phenomenon further revealed the efficient adsorption and distinct decolouration for tinctorial wastewater using PCNS. Specifically, about 95% of MB was removed by PCNS during the first 10 min of adsorption, while only a small portion of the additional removal occurred during the rest of time.

Table 2 Comparison of the adsorption capacity of MB onto various adsorbents.

Adsorbent	Adsorption capacity (mg/g)	Reference
CNS	30.3	This work
Graphene nanosheet	111.62	17
Activated CS-CNT	172.4	18
Ni/C nanomaterial	175.2	19
BN hollow sphere	191.7	20
Ni nanosphere	250	21
Porous MnO ₂ microsphere	259.2	22
Montmorillonite	300.3	23
Activated CNT	400	24
Activated carbon	452.2	25
CNS	585	69
Ordered mesoporous carbon	758	26
PCNS	769.2	This work
CNF aerogel	800	28

65

The recyclability and reusability of adsorbent are very important to its practical applications. In this study, the regeneration of PCNS after MB adsorption is conducted by thermal annealing under Ar atmosphere. Fig. 9a shows the adsorption performance of reclaimed PCNS. The adsorption capacity of PCNS after five cycles was 734.4 mg/g, which was approximately 96% of the original capacity (761.1 mg/g). After ten cycles, PCNS still performed excellently with the adsorption capacity of 692.0 mg/g in removal of MB, which was

approximately 91% of the original capacity. These values were still higher than many of those reported adsorbents (Table 2). Besides, after ten cycles, about 90 wt % of PCNS was recovered.

As well known, adsorption reaction may lead to changes in the phase and textural structures of the adsorbent, and hence the understanding of the resulting structure changes of the adsorbent during adsorption could provide valuable information regarding adsorption mechanism. XRD patterns taken before and after MB adsorption are thus displayed in Fig. 9b, which indicated no appreciable changes in the patterns, and no other peaks corresponding to impurities were detected. This suggested that the MB molecules adsorbed by PCNS did not alter the phase structure of PCNS, that is to say, the adsorption was physical in nature.

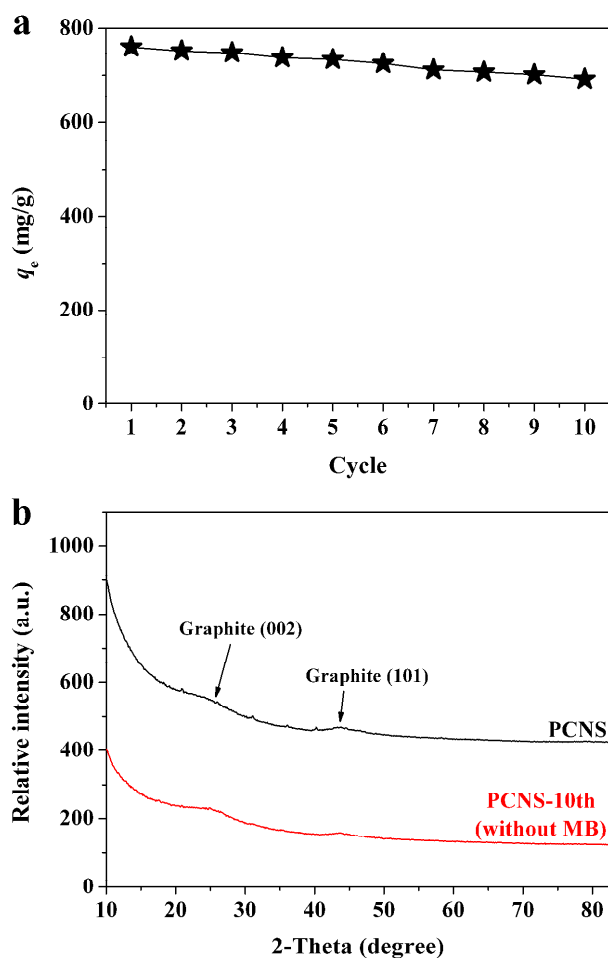


Fig. 9 (a) The reusability of PCNS for the adsorption of MB (Experimental conditions: MB concentration = 400 mg/L, PCNS concentration = 0.5 g/L, and adsorption time = 180 min), and (b) XRD patterns of PCNS before and after ten cycles.

Table 3 Textural parameters of PCNS, PCNS-1st (with MB) and PCNS-10th (without MB).

Property	PCNS	PCNS-1st (with MB)	PCNS-10th (without MB)
S_{BET} (m^2/g)	2315.0	1078.0	1990.2
V (cm^3/g)	3.319	1.792	2.854
D_{AV} (nm)	3.83	3.82	3.82

As a result, the decrease of the adsorption capacity after ten cycles may probably be ascribed to the textural change of PCNS. To confirm this speculation, nitrogen adsorption/desorption measurements are used to characterize the change of pore structures of PCNS before and after MB adsorption. As presented in Fig. 10, the nitrogen adsorption/desorption isotherms of the original, used and recycled PCNS were similar in shape. The hysteresis in the relative pressure range of 0.4–1.0 was maintained with similar pore size distributions. As shown in Table 3, after the adsorption of MB (the first cycle), the S_{BET} and V of PCNS decreased from 2315.0 to 1078.0 m^2/g , and from 3.319 to 1.792 cm^3/g , respectively, which were explained as that mesopores favored for the adsorbate-adsorbate interaction *via* mesopore filling mechanism. Besides, one could see that the nitrogen adsorption/desorption isotherm and pore size distribution of the regenerated PCNS (PCNS-10th) were quite similar to those of the original PCNS. However, the slight decreases of S_{BET} and V of the PCNS-10th were observed, which were probably attributed to the deposition of MB molecules on the PCNS surface during thermal annealing.

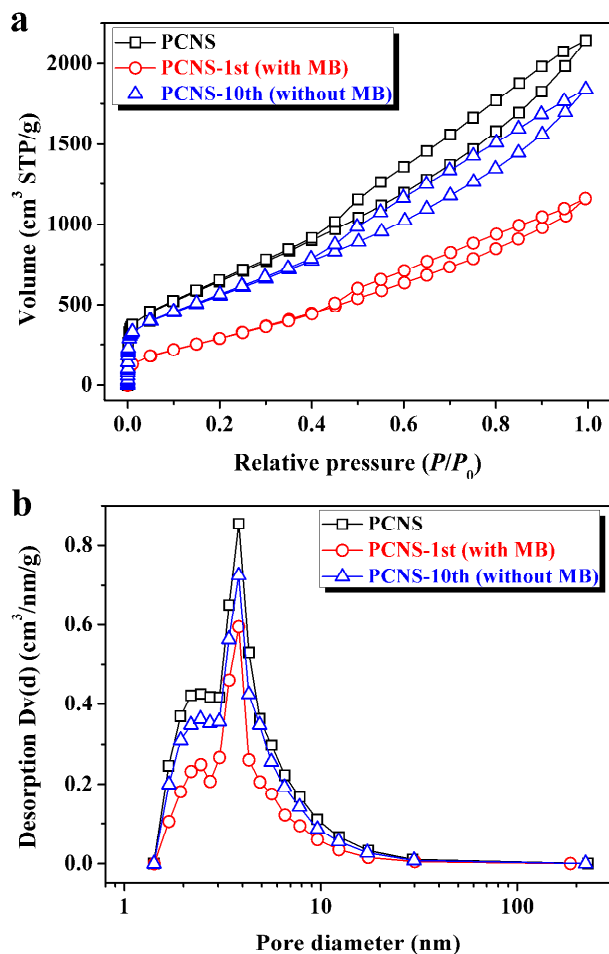


Fig. 10 Nitrogen adsorption/desorption isotherms (a) and pore size distributions (b) of PCNS before and after MB adsorption (the first cycle), and PCNS after ten cycles.

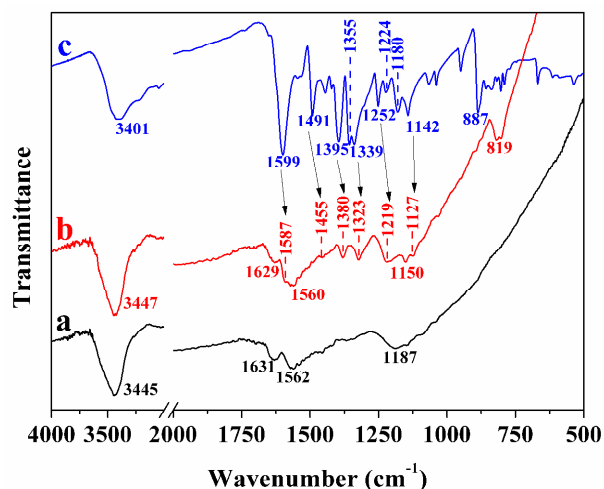


Fig. 11 FT-IR spectra of PCNS before (a) and after (b) adsorption of MB, and pure MB (c).

After adsorbed by PCNS, obvious shifts were observed to 1587 and 1380 cm⁻¹ for C=N (and C=C) and C-N bonds in the heterocycle of MB and to 1455 cm⁻¹ for CH₂ deformation vibration in benzene ring (Fig. 11b), which corresponded to the attachment of MB on the surface of PCNS by π - π stacking interaction between the aromatic backbone of MB and hexagonal skeleton of PCNS, since MB is an ideally planar molecule. This could be further proved by the appearance of a new band (819 cm⁻¹), which was ascribed to wagging vibration of C-H in aromatic ring of MB. Besides, the peaks associated with the C-N bond connected with benzene ring and N-CH₃ bond, the Ar-N deformation vibration and the stretching vibrations of C=S and C-S were broadened with significant decreases in intensity and shifted to 1323, 1219, 1150 and 1127 cm⁻¹, respectively. This suggested that the nitrogen atom of C-N group and sulfur atom of C-S group could be used as the hydrogen-bonding acceptor and formed intramolecular hydrogen bonding with the hydrogen atom of the hydroxyl group of PCNS, since MB is a kind of cationic dye which can be adsorbed easily by electrostatic forces on negatively charged surfaces.

As a consequence, the excellent performance of PCNS in the adsorption of MB resulted from the high specific surface area and large pore volume of PCNS, and multiple adsorption interaction mechanisms including pore filling, hydrogen bonding, π - π and electrostatic interactions between MB and PCNS as schematically illustrated in Fig. 12.

FT-IR spectra of PCNS before and after adsorption of MB, and pure MB are analyzed to gain more insights into the adsorption mechanism. FT-IR spectrum of PCNS (Fig. 11a) confirmed the presence of functional groups, including -OH (3445 cm⁻¹), -C=C- (1631 cm⁻¹), -C=O (1562 cm⁻¹) and -C-O- (1187 cm⁻¹), which not only led to the hydrophilic nature of PCNS but also acted as anchoring sites for MB molecules. In the case of MB (Fig. 11c), the peaks at 1599 and 1395 cm⁻¹ were assigned to the stretching vibrations of C=N (and C=C) and C-N bonds in the heterocycle of MB, respectively, while the peaks at 1355 and 1339 cm⁻¹ were attributed to the stretching vibration of C-N bond connected with benzene ring and N-CH₃ bond. The band at about 1491 cm⁻¹ was ascribed to the CH₂ deformation vibration, while the band around 1395 cm⁻¹ was owing to the CH₃ deformation vibration. Furthermore, the bands at about 1252 and 1224 cm⁻¹ were due to Ar-N deformation vibration, the bands around 1180 and 1142 cm⁻¹ to the stretching vibrations of C=S and C-S, and the band around 887 cm⁻¹ to the wagging vibration of C-H in aromatic ring of MB.

25

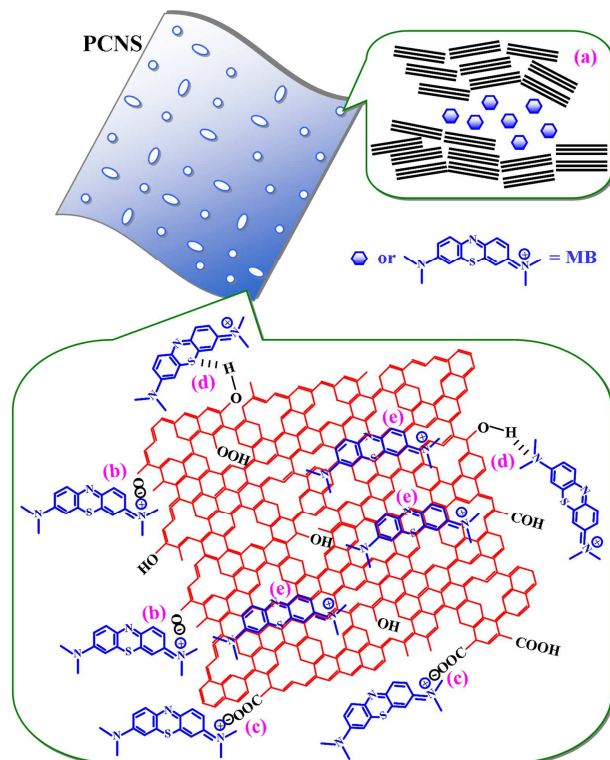


Fig. 12 Schematic illustration of the interactions between PCNS and MB: (a) pore filling, (b) and (c) electrostatic attraction, (d) hydrogen bonding and (e) π - π interactions.

5

From the above results, it is clear that our method shows several advantages. Firstly, the carbon feedstock for the synthesis of PCNS comes from the “real-world” mixed waste plastics, which are rather cheap and easy available. To the best of our knowledge, this is the first report to convert “real-world” mixed waste plastics into PCNS. Secondly, our work contributes to the sustainable development. This is because most of waste plastics from the unsustainable fossil fuels are not biodegradable, which have created environmental pollutions (such as “white pollution”). Thirdly, the proposed method is facile and easily operated. At last, the resultant PCNS displays excellent performance in the adsorption of MB from wastewater, demonstrating its potential application in wastewater treatment.

15

Besides, since continuous adsorption in fixed-bed columns can be easily scaled up and is simple to operate and also more beneficial than batch adsorption from an industrial point of view, more investigations about the column adsorption studies of PCNS for real samples will be conducted in the future work.

Conclusions

We successfully converted the “real-world” mixed waste plastics containing PP, PE and PS into high value-added PCNS using a facile approach. PCNS had randomly oriented lattice fringes and displayed the layered morphology consisting of thin, leaf-like nanosheets ranging from hundreds of nanometers to several micrometers in length. Besides, PCNS showed high specific surface area (2315.0 m^2/g) and large pore volume (3.319 cm^3/g) with high purity and abundant surface functional groups. More importantly, it was demonstrated that PCNS exhibited fast

30

adsorption, unprecedented adsorption capacity of 769.2 mg/g (higher than most of reported adsorbents) and excellent recyclability (after ten cycles, adsorption capacity of 692.0 mg/g was remained, and 90 wt % of PCNS was recovered) for removal of MB from wastewater. This resulted from the high specific surface area and large pore volume of PCNS, and the multiple adsorption mechanisms including pore filling, hydrogen bonding, π - π and electrostatic interactions between MB and PCNS. That is to say, PCNS showed to be a promising adsorbent for practical applications. It should be worth noting that the gas and liquid products of the “real-world” mixed waste plastics (e.g., hydrogen, propylene and benzene) during the formation of CNS could be used as important chemical raw materials. It is believed that this work not only opens up a novel way to recycle waste plastics, but also puts forward a facile sustainable approach to synthesize PCNS, which will be an ideal candidate for many applications such as environment remediation, energy storage and catalysis, etc. The related investigations are on the way in our laboratory.

Acknowledgements

We would like to thank the reviewers for kind and important suggestions. This work was supported by the National Natural Science Foundation of China (51373171, 21204079, 51233005 and 21374114) and Polish Foundation (No. 2011/03/D/ST5/06119).

Notes and references

^a State Key Laboratory of Polymer Physics and Chemistry, Changchun Institute of Applied Chemistry, Chinese Academy of Sciences, Changchun 130022, China. Fax: +86 (0) 431 85262827; Tel: +86 (0) 431 85262004; E-mail: ttang@ciac.ac.cn

^b University of Chinese Academy of Sciences, Beijing 100049, China
^c Institute of Chemical and Environment Engineering, West Pomeranian University of Technology, Szczecinul. Pulaskiego 10, 70-322 Szczecin, Poland

† Electronic Supplementary Information (ESI) available: Schematic diagram of the carbonization of the “real-world” mixed waste plastics/OMMT to prepare CNS/MMT composite; XPS spectra of CNS and PCNS; the removal efficiency of MB by PCNS in the different environment. See DOI: 10.1039/b000000x/

References

- V. K. Gupta, R. Jain, A. Mittal, T. A. Saleh, A. Nayak, S. Agarwal and S. Sikarwar, *Mat. Sci. Eng. C*, 2012, **32**, 12–17.
- T. A. Saleh and V. K. Gupta, *Environ. Sci. Pollut. Res.*, 2012, **19**, 1224–1228.
- V. K. Gupta, S. K. Srivastava, D. Mohan and S. Sharma, *Waste Manage.*, 1997, **17**(8), 517–522.
- V. K. Gupta, S. Agarwal and T. A. Saleh, *J. Hazard. Mater.*, 2011, **185**, 17–23.
- V. K. Gupta, I. Ali, T. A. Saleh, A. Nayak and S. Agarwal, *RSC Adv.*, 2012, **2**, 6380–6388.
- V. K. Gupta, R. Jain, A. Nayak, S. Agarwal and M. Shrivastava, *Mat. Sci. Eng. C*, 2011, **31**, 1062–1067.
- V. K. Gupta and A. Nayak, *Chem. Eng. J.*, 2012, **180**, 81–90.
- T. A. Saleh and V. K. Gupta, *J. Colloid Interf. Sci.*, 2012, **371**, 101–106.
- H. Khani, M. K. Rofouei, P. Arab, V. K. Gupta and Z. Vafaei, *J. Hazard. Mater.*, 2010, **183**, 402–409.
- S. Karthikeyan, V. K. Gupta, R. Boopathy, A. Titus and G. Sekaran, *J. Mol. Liq.*, 2012, **173**, 153–163.
- A. Mittal, J. Mittal, A. Malviya, D. Kaur and V. K. Gupta, *J. Colloid Interf. Sci.*, 2010, **342**, 518–527.

- 12 A. Mittal, D. Kaur, A. Malviya, J. Mittal and V. K. Gupta, *J. Colloid Interf. Sci.*, 2009, **337**, 345–354.
- 13 A. Mittal, J. Mittal, A. Malviya and V. K. Gupta, *J. Colloid Interf. Sci.*, 2009, **340**, 16–26.
- 5 14 A. Mittal, J. Mittal, A. Malviya and V. K. Gupta, *J. Colloid Interf. Sci.*, 2010, **344**, 497–507.
- 15 A. K. Jain, V. K. Gupta, A. Bhatnagar and Suhas, *Sep. Sci. Technol.*, 2003, **38(2)**, 463–481.
- 16 M. M. Khin, A. S. Nair, V. J. Babu, R. Murugan and S. Ramakrishna, *Energy Environ. Sci.*, 2012, **5**, 8075–8109.
- 10 17 Z. J. Fan, W. Kai, J. Yan, T. Wei, L. J. Zhi, J. Feng, Y. M. Ren, L. P. Song and F. Wei, *ACS Nano*, 2011, **5(1)**, 191–198.
- 18 J. Gong, J. D. Feng, J. Liu, Z. W. Jiang, X. C. Chen, E. Mijowska, X. Wen and T. Tang, *Chem. Eng. J.*, 2014, **248**, 27–40.
- 15 19 J. Gong, K. Yao, J. Liu, X. Wen, X. C. Chen, Z. W. Jiang, E. Mijowska and T. Tang, *Chem. Eng. J.*, 2013, **215–216**, 339–347.
- 20 G. Lian, X. Zhang, S. J. Zhang, D. Liu, D. L. Cui and Q. L. Wang, *Energy Environ. Sci.*, 2012, **5**, 7072–7080.
- 21 A. Ghosal, J. Shah, R. K. Kotnala and S. Ahmad, *J. Mater. Chem. A*, 2013, **1**, 12868–12878.
- 20 22 R. Chen, J. Yu and W. Xiao, *J. Mater. Chem. A*, 2013, **1**, 11682–11690.
- 23 C. A. P. Almeida, N. A. Debacher, A. J. Downs, L. Cottet and C. A. D. Mello, *J. Colloid Interf. Sci.*, 2009, **332**, 46–53.
- 25 24 J. Ma, F. Yu, L. Zhou, L. Jin, M. X. Yang, J. S. Luan, Y. H. Tang, H. B. Fan, Z. W. Yuan and J. H. Chen, *ACS Appl. Mater. Interfaces*, 2012, **4**, 5749–5760.
- 25 B. H. Hameed, A. T. M. Din and A. L. Ahmad, *J. Hazard. Mater.*, 2007, **141**, 819–825.
- 30 26 X. Zhuang, Y. Wan, C. M. Feng, Y. Shen and D. Y. Zhao, *Chem. Mater.*, 2009, **21**, 706–716.
- 27 W. Teng, Z. X. Wu, J. W. Fan, H. Chen, D. Feng, Y. Y. Lv, J. X. Wang, A. M. Asirid and D. Y. Zhao, *Energy Environ. Sci.*, 2013, **6**, 2765–2776.
- 35 28 H. W. Liang, Q. F. Guan, L. F. Chen, Z. Zhu, W. J. Zhang and S. H. Yu, *Angew. Chem. Int. Ed.*, 2012, **124**, 5191–5195.
- 29 H. W. Liang, X. Cao, W. J. Zhang, H. T. Lin, F. Zhou, L. F. Chen, and S. H. Yu, *Adv. Funct. Mater.*, 2011, **21**, 3851–3858.
- 30 S. Y. Sawant, R. S. Somani, S. S. Sharma and H. C. Bajaj, *Carbon*, 2014, **68**, 2100–2200.
- 40 31 Q. Wen, S. Y. Wang, J. Yan, L. J. Cong, Y. Chen and H. Y. Xi, *Bioelectrochemistry*, 2014, **95**, 23–28.
- 32 J. S. Lee, H. I. Joh, T. W. Kim and S. Lee, *Org. Electron.*, 2014, **15**, 132–138.
- 45 33 Y. C. Wang and X. E. Jiang, *ACS Appl. Mater. Interfaces*, 2013, **5**, 11597–11602.
- 34 Plastics—the Facts 2013, An analysis of European latest plastics production, demand and waste data, Brussels, 2013.
- 35 R. Luque, L. Herrero-Davila, J. M. Campelo, J. H. Clark, J. M. Hidalgo, D. Luna, J. M. Marinas and A. A. Romero, *Energy Environ. Sci.*, 2008, **1**, 542–564.
- 50 36 M. M. Titirici and M. Antonietti, *Chem. Soc. Rev.*, 2010, **39**, 103–116.
- 37 B. Hu, K. Wang, L. H. Wu, S. H. Yu, M. Antonietti and M. M. Titirici, *Adv. Mater.*, 2010, **22**, 813–828.
- 55 38 J. A. Melero, J. Iglesias and A. Garcia, *Energy Environ. Sci.*, 2012, **5**, 7393–7420.
- 39 M. M. Titirici, R. J. White, C. Falco and M. Sevilla, *Energy Environ. Sci.*, 2012, **5**, 6796–6822.
- 40 M. Biswal, A. Banerjee, M. Deo and S. Ogale, *Energy Environ. Sci.*, 2013, **6**, 1249–1259.
- 60 41 C. S. K. Lin, L. A. Pfaltzgraff, L. Herrero-Davila, E. B. Mubofu, S. Abderrahim, J. H. Clark, A. A. Koutinas, N. Kopsahelis, K. Stamatelatou, F. Dickson, S. Thankappan, Z. Mohamed, R. Brocklesby and R. Luque, *Energy Environ. Sci.*, 2013, **6**, 426–464.
- 65 42 O. Eriksson and G. Finnveden, *Energy Environ. Sci.*, 2009, **2**, 907–914.
- 43 B. Baytekin, H. T. Baytekin and B. A. Grzybowski, *Energy Environ. Sci.*, 2013, **6**, 3467–3482.
- 44 P. T. Williams and E. Slaney, *Resour. Conserv. Recycl.*, 2007, **51**, 754–769.
- 70 45 D. P. Serrano, J. Aguado and J. M. Escola, *ACS Catal.*, 2012, **2**, 1924–1941.
- 46 C. F. Wu, M. A. Nahil, N. Miskolczi, J. Huang and P. T. Williams, *Environ. Sci. Technol.*, 2014, **48**, 819–826.
- 47 J. C. Acomb, C. F. Wu and P. T. Williams, *Appl. Catal. B: Environ.*, 2014, **147**, 571–584.
- 75 48 C. W. Zhuo, B. Hall, H. Richter and Y. Levendis, *Carbon*, 2010, **48**, 4024–4034.
- 49 V. G. Pol and M. M. Thackeray, *Energy Environ. Sci.*, 2011, **4**, 1904–1912.
- 80 50 V. G. Pol, *Environ. Sci. Technol.*, 2010, **44**, 4753–4759.
- 51 L. Z. Wei, N. Yan and Q. W. Chen, *Environ. Sci. Technol.*, 2011, **45(2)**, 534–539.
- 52 G. D. Ruan, Z. Z. Sun, Z. W. Peng and J. M. Tour, *ACS Nano*, 2011, **5(9)**, 7601–7607.
- 85 53 T. Tang, X. C. Chen, X. Y. Meng, H. Chen and Y. P. Ding, *Angew. Chem. Int. Ed.*, 2005, **44**, 1517–1520.
- 54 Z. W. Jiang, R. J. Song, W. G. Bi, J. Lu and T. Tang, *Carbon*, 2007, **45**, 449–458.
- 90 55 R. J. Song, Z. W. Jiang, W. G. Bi, W. X. Cheng, J. Lu, B. T. Huang and T. Tang, *Chem. Eur. J.*, 2007, **13**, 3234–3240.
- 56 J. Gong, J. Liu, L. Ma, X. Wen, X. C. Chen, D. Wan, H. O. Yu, Z. W. Jiang, E. Borowiak-Palen and T. Tang, *Appl. Catal. B: Environ.*, 2012, **117–118**, 185–193.
- 95 57 J. Gong, J. Liu, D. Wan, X. C. Chen, X. Wen, E. Mijowska, Z. W. Jiang, Y. H. Wang and T. Tang, *Appl. Catal. A: Gen.*, 2012, **449**, 112–120.
- 58 J. Gong, J. Liu, Z. W. Jiang, J. D. Feng, X. C. Chen, L. Wang, E. Mijowska, X. Wen and T. Tang, *Appl. Catal. B: Environ.*, 2014, **147**, 592–601.
- 100 59 J. Gong, J. Liu, Z. W. Jiang, X. C. Chen, X. Wen, E. Mijowska and T. Tang, *Appl. Catal. B: Environ.*, 2014, **152–153**, 289–299.
- 60 C. F. Wu and P. T. Williams, *Fuel*, 2010, **89**, 3022–3032.
- 61 Z. J. Fan, Y. Liu, J. Yan, G. Q. Ning, Q. Wang, T. Wei, L. J. Zhi and F. Wei, *Adv. Energy Mater.*, 2012, **2**, 419–424.
- 105 62 X. Zhao, H. Tian, M. Y. Zhu, K. Tian, J. J. Wang, F. Y. Kang and R. A. Outlaw, *J. Power Sources*, 2009, **194**, 1208–1212.
- 63 S. Y. Son, Y. J. Noh, C. Bok, S. Lee, B. G. Kim, S. I. Na and H. I. Joh, *Nanoscale*, 2014, **6**, 678–682.
- 110 64 Y. Fang, Y. Y. Lv, R. C. Che, H. Y. Wu, X. H. Zhang, D. Gu, G. F. Zheng and D. Y. Zhao, *J. Am. Chem. Soc.*, 2013, **135**, 1524–1530.
- 65 J. T. Zhang, Z. Y. Jin, W. C. Li, W. Dong and A. H. Lu, *J. Mater. Chem. A*, 2013, **1**, 13139–13145.
- 66 G. P. Hao, Z. Y. Jin, Q. Sun, X. Q. Zhang, J. T. Zhang and A. H. Lu, *Energy Environ. Sci.*, 2013, **6**, 3740–3747.
- 115 67 Z. Y. Jin, A. H. Lu, Y. Y. Xu, J. T. Zhang and W. C. Li, *Adv. Mater.*, 2014, **26(22)**, 3700–3705.
- 68 D. J. Cott, M. Verheijen, O. Richard, I. Radu, S. D. Gendt, S. van Elshocht and P. M. Vereecken, *Carbon*, 2013, **58**, 59–65.
- 120 69 W. T. Wang, S. Chakrabarti, Z. G. Chen, Z. F. Yan, M. O. Tade, J. Zoudf and Q. Li, *J. Mater. Chem. A*, 2014, **2**, 2390–2396.
- 70 J. Gong, J. Liu, X. Wen, Z. W. Jiang, X. C. Chen, E. Mijowska and T. Tang, *Ind. Eng. Chem. Res.*, 2014, **53**, 4173–4181.
- 71 Y. Zhu, S. Murali, M. D. Stoller, K. J. Ganesh, W. Cai, P. J. Ferreira, A. Pirkle, R. M. Wallace, K. A. Cychoz, M. Thommes, D. Su, E. A. Stach and R. S. Ruoff, *Science*, 2011, **332**, 1537–1541.
- 125 72 J. C. Wang and S. Kaskel, *J. Mater. Chem.*, 2012, **22**, 23710–23725.
- 73 Y. Dong, H. M. Lin, Q. M. Jin, L. Li, D. Wang, D. Zhou and F. Y. Qu, *J. Mater. Chem. A*, 2013, **1**, 7391–7398.
- 130 74 M. H. Rummeli, A. Bachmatiuk, A. Scott, F. Börrnert, J. H. Warner, V. Hoffman, J. H. Lin, G. Cuniberti and B. Büchner, *ACS Nano*, 2010, **4(7)**, 4206–4210.
- 75 J. Gong, J. Liu, X. C. Chen, Z. W. Jiang, X. Wen, E. Mijowska and T. Tang, *J. Mater. Chem. A*, 2014, **2**, 7461–7470.
- 135 76 R. Demir-Cakan, N. Baccile, M. Antonietti and M. M. Titirici, *Chem. Mater.*, 2009, **21**, 484–490.

Table of Contents (TOC)

Converting “real-world” mixed waste plastics into porous carbon nanosheet with excellent performance in adsorption of organic dye from wastewater

5 Jiang Gong, Jie Liu, Xuecheng Chen, Zhiwei Jiang, Xin Wen, Ewa Mijowska and Tao Tang*

“Real-world” mixed waste plastics were converted into PCNS, which exhibited fast adsorption, unprecedented adsorption capacity and excellent recyclability for MB.

10

